ISSN: 2836-3655
DOI: 10.33552/AHM.2024.01.000523
Advances in Hydrology & Meteorology
Iris Publishers

Research Article

Improving Low-Frequency Flood Estimation Using the Partial Duration Series Instead of the Annual Maximum Across the United States

Rouzbeh Berton[1]* and Vahid Rahmani[2]

[1]*Rouzbeh Berton, Senior Associate Civil Engineer, Hydrology and Hydraulics, Stantec Consulting Inc., 410 17th St #1400, Denver, Colorado, USA*

[2]*Vahid Rahmani, Adjunct Faculty, Kansas State University, 1016 Seaton Hall, 920 N. 17th Street, Manhattan, Kansas, USA*

***Corresponding author:** Rouzbeh Berton, Senior Associate Civil Engineer, Hydrology and Hydraulics, Stantec Consulting Inc., 410 17th St #1400, Denver, Colorado, USA.

Received Date: June 10, 2024

Published Date: June 21, 2024

Abstract

Reliable flood forecasting is crucial for minimizing infrastructure damage and fatalities. Utilizing multiple independent peak flow observations throughout the year, rather than solely relying on the annual maximum, can enhance flood estimation accuracy. Some studies have incorporated the partial duration series (PDS) alongside the annual maximum flood (AMF) to better estimate floods across the United States. With wet years expected to become wetter, independent high flow events within wet years may surpass the AMF of dry years. Given that global climate warming can exacerbate flooding, integrating several independent peak flow observations with the AMF could address nonstationarity in flood analysis more effectively.

We applied two common univariate distributions, namely Log Pearson Type III (LP3) and Generalized Extreme Value (GEV), to fit the AMF and PDS data. However, a high correlation between observed and estimated flood quantiles could potentially mislead us into confirming the reliable performance of LP3 or GEV. Therefore, in addition to conducting goodness-of-fit tests, we introduced the ratio (R) of observed to estimated flood values to provide a better evaluation of distribution performance. When R fell below one, it indicated that estimated floods equaled or exceeded the observations, suggesting reliable performance. Conversely, when R exceeded one, the distribution did not perform reliably.

Our study demonstrated regional improvements in estimating floods with return intervals ranging from two to 400 years when LP3 or GEV were fitted to the PDS rather than the AMF. We examined both reference and non-reference sites across the U.S. with over 100 years of AMF data. We found that LP3 performed reliably for two-to-10-year floods, regardless of whether it was fitted to the AMF or PDS. However, the GEV showed better performance in estimating high flood quantiles ranging from 50 to 400 years when fitted to the PDS. The findings of this research have significant implications for enhancing the sustainable design of infrastructure, particularly for non-reference sites experiencing both climate change and anthropogenic disturbances.

Keywords: NONSTATIONARITY IN PEAK FLOW; PARTIAL DURATION SERIES (PDS); ANNUAL MAXIMUM FLOOD (AMF); LOG PEARSON TYPE III (LP3); GENERALIZED EXTREME VALUE (GEV); UNITED STATES

Introduction

Minimizing the risk of infrastructure damage and fatalities from flooding requires reliable estimates of flood quantiles [1-6]. Achieving reliable flood estimation remains a challenge in the era of nonstationary climate and anthropogenically manipulated

watersheds that have experienced land use/cover change, water diversion, and/or damming [7-9]. In nonstationary conditions, every unit change in climate or anthropogenic disturbances necessarily does not correspond to a unit change in peak flow [10-15]. Hence, considering multiple independent peak flow observations throughout the year, alongside the annual maximum, can improve flood estimation accuracy [16, 17].

Limited studies have incorporated the partial duration series (PDS) alongside the annual maximum flood (AMF) to estimate flood quantiles across the U.S. [18-23]. With wet years expected to become wetter [24, 25], a second or subsequent larger flow in a wet year can easily surpass the AMF in a dry year [26, 16]. Combining several independent flooding events per year with an AMF is likely to enhance flood quantile estimates, both at high and low ends, depending on the degree of watershed disturbance [19, 26-30].

Several studies have distinguished between reference and nonreference gauging stations on flood analysis across the U.S. [31-33, 30, 34]. Reference stations measure streamflow within minimally disturbed watersheds, while nonreference stations are located within watersheds with regulated streams, manmade reservoirs, water withdrawal, and/or changes in land use/cover. Studying peak flow at reference sites provides insight into how climate variation and change may affect flood quantile estimates. Conversely, the peak flow information of nonreference sites helps demonstrate how flood estimates may change under concurrent influences of changing climate and anthropogenic disturbances [35, 36].

The Log Pearson Type III (LP3) has been widely recommended as a suitable statistical distribution for analyzing flood frequency across the U.S. [37, 7, 26, 38, 39]. The LP3 distribution typically utilizes the AMF as an input [40- 42, 29]. However, as mentioned earlier, flood quantile estimates with LP3 fitted to the AMF sometimes fail to capture all observed peak flows. In such cases, using a PDS with the Generalized Extreme Value (GEV) distribution may offer improved flood quantile estimates [19, 23, 16, 27, 30].

In the following study, we aim to accomplish two main objectives: 1) develop a PDS using daily streamflow data for sites with more than 100 years of AMF records, and 2) demonstrate that the GEV distribution combined with the PDS yields better performance than the LP3 distribution with AMF for estimating flood quantiles. The reliability of flood analysis can vary geographically between reference and nonreference sites. We constructed PDSs for 24 reference and 75 nonreference sites across the U.S., each having more than 100 years of AMF observations. LP3 and GEV distributions were fitted to both the AMF and PDS to estimate floods with return periods ranging from two to 400 years. This study emphasize the advantages of incorporating the PDS into flood forecasting alongside the AMF, particularly for reference sites compared to nonreference sites. The findings of this research hold significant potential for enhancing the sustainable design of water infrastructures for regions undergoing both changing climate and anthropogenic disturbances.

Materials and Methods

LP3 and GEV are extensively utilized statistical distributions for estimating flood quantiles [17, 29]. The distribution parameters can be computed using either product or linear moment methods [43]. Typically, the parameters of the LP3 distribution are approximated using the product moment method, while those of the GEV distribution are estimated using the linear moment method [41]. In this study, we followed the LP3 and GEV formulations outlined by [44], which are briefly summarized in this section. We employed station-based skewness without applying any regional correction and developed an "R" code to compute LP3 and GEV distribution parameters.

Log Pearson Type III (LP3)

The Probability Density Function (PDF) of LP3 distribution can be expressed as follows:

$$f_x(X) = |\beta| \left[\beta\left(\ell n\left(X\right)-\xi\right)\right]^{\alpha-1} \frac{exp\left[-\beta\left(\ell n\left(X\right)-\xi\right)\right]}{X\Gamma\left(\alpha\right)}, X = \ell n(Q) \quad \text{Eq.(1)}$$

The descriptive statistics of peak flow observations, including the mean ($\hat{\mu}_X$, first moment), variance ($\hat{\sigma}_X^2$, second moment), and skewness ($\hat{\gamma}_X$, third moment) (Eq. 2), are used to calculate the distribution parameters of shape (α), scale (β), and location (ξ):

$$\hat{\mu}_X = \bar{X} = \frac{1}{n}\sum_{i=1}^{n} X_i, \hat{\sigma}_X^2 = S^2 = \frac{1}{n-1}\sum_{i=1}^{n}(X_i - \bar{X})^2,$$

$$\hat{\gamma}_X = \frac{n}{(n-1)(n-2)S^3}\sum_{i=1}^{n}(X_i - \bar{X})^3 \quad \text{Eq.(2)}$$

$$\alpha = \frac{4}{\hat{\gamma}_X^2}, \beta = \frac{2}{\hat{\sigma}_X\hat{\gamma}_X}, \xi = \hat{\mu}_X - \frac{\alpha}{\beta} = \hat{\mu}_X - \frac{2\hat{\sigma}_X}{\hat{\gamma}_X} \quad \text{Eq.(3)}$$

Subsequently, the flood quantiles will be estimated as follows:

$$X_p = \mu_Q + \sigma_Q K_P(\gamma_Q) \text{ where Eq(4)}$$

$$\mu_Q = e^{\xi}\left(\frac{\beta}{\beta-1}\right)^2, \sigma_Q^2 = e^{2\xi}\left[\left(\frac{\beta}{\beta-2}\right)^{\alpha} - \left(\frac{\beta}{\beta-1}\right)^{2\alpha}\right], E\left[Q^r\right] = e^{r\xi}\left(\frac{\beta}{\beta-r}\right)^{\alpha},$$

$$\gamma_Q = \frac{E\left[Q^3\right] - 3\mu_Q E\left[Q^2\right] + 2\mu_Q^3}{\sigma_Q^3}, K_P\left(\gamma_Q\right) = \frac{2}{\gamma_Q}\left[1 + \frac{\gamma_Q Z_P}{6} - \frac{\gamma_Q^2}{36}\right] - \frac{2}{\gamma_Q}$$

Z_P corresponds to the P[th] quantiles of the standard normal distribution, numerically estimated by the following equation:

$$Z_P = \frac{P^{0.135} - (1-P)^{0.135}}{0.1975} \text{ for } P > 0.5 \text{ Eq.(5)}$$

The goodness of fit is verified using the Blom empirical probability formula [45]:

$$P_i = 1 - \frac{i - 0.375}{n + 0.25} \text{ Eq. (6)}$$

where $i = 1$ corresponds to the greatest observation ranked and "n" is the total number of peak flow observations. When the plot of $K_{P_i}\left(\gamma_Q\right)$ against the anomaly of observations $Z_i = \frac{X_i - \bar{X}}{\sigma_X}$ falls on the 1:1 line, LP3 reliably estimates flood quantiles [29].

Generalized Extreme Value (GEV)

The GEV distribution is represented by the following Cumulative Distribution Functions (CDF):

$$F_X(X) = exp\left\{-\left[1 - \frac{\kappa(X-\xi)}{\alpha}\right]^{\frac{1}{k}}\right\} \text{ Eq. (7)}$$

where X represents sorted observations from largest to smallest. The three L-moment estimators of $\hat{\lambda}_1(k)$, $\hat{\lambda}_2(k)$, and $\hat{\lambda}_3(k)$ can be calculated as follows:

$$\hat{\lambda}_1 = \hat{\beta}_0,\ \hat{\lambda}_2 = 2\hat{\beta}_1 - \hat{\beta}_0,\ \hat{\lambda}_3 = 6\hat{\beta}_1 - 6\hat{\beta}_1 + \beta \quad \text{where Eq. (8)}$$

$$\hat{\beta}_0 = \bar{X}\ ,\ \hat{\beta}_1 = \sum_{j=1}^{n-1}\frac{(n-j)X_j}{n(n-1)}\ ,\ \hat{\beta}_2 = \sum_{j=1}^{n-2}\frac{(n-j)(n-j-1)X_j}{n(n-1)(n-2)}$$

Then the flood quantiles are computed by GEV distribution:

$$\hat{X}_p = \xi + \frac{\alpha}{\kappa}\left\{1 - \left[-\ell nP\right]^{\kappa}\right\} \text{ where } c = \frac{2\hat{\lambda}_2}{\hat{\lambda}_3 + 3\hat{\lambda}_2} - \frac{\ell n2}{\ell n3}, \kappa = 7.8590c + 2.9554c^2\ ,$$

$$\sigma = \frac{\kappa\hat{\lambda}_2}{\left(1 - 2^{-\kappa}\right)\Gamma(1+\kappa)}\ ,\ \xi = \hat{\lambda}_1 - \frac{\alpha}{\kappa}\left[1 - \Gamma(1+\kappa)\right] \text{ Eq. (9)}$$

The visual goodness-of-fit test is developed by plotting $\hat{X}_{P_i}$ against the peak flow anomaly $Z_i = \frac{X_i - \bar{X}}{\sigma_X}$ fallen on the 1:1 line with the best fit [29]. The term is computed using Cunnane's empirical probability [46]:

$$P_i = 1 - \frac{i - 0.4}{n + 0.2} \quad \text{Eq. (10)}$$

where $i = 1$ for the greatest observation.

Data

Annual maximum flood (AMF)

Among 9,067 USGS gauging stations, we selected 99 stations that have more than 100 years of AMF information. Using data from the "Hydro-Climatic Data Network" (HCDN or Gages-II) [47], we classified 24 sites as reference sites situated in undisturbed watersheds, while the remaining 75 were categorized as nonreference sites located in disturbed watersheds. Reference sites experience minimal or no anthropogenic disturbances, whereas nonreference sites exhibit varying levels of land use/cover change, river regulation, and/or reservoir construction [48]. The geographical distribution of stream gauges is illustrated on Figure 1, with additional detailed information about the study sites provided in supplementary materials Table S1. Daily streamflow and peak flow data were obtained from the USGS National Water Information System (NWIS) data repository using the "dataRetrieval" [49] and "dplyr" [50] packages developed in "R."

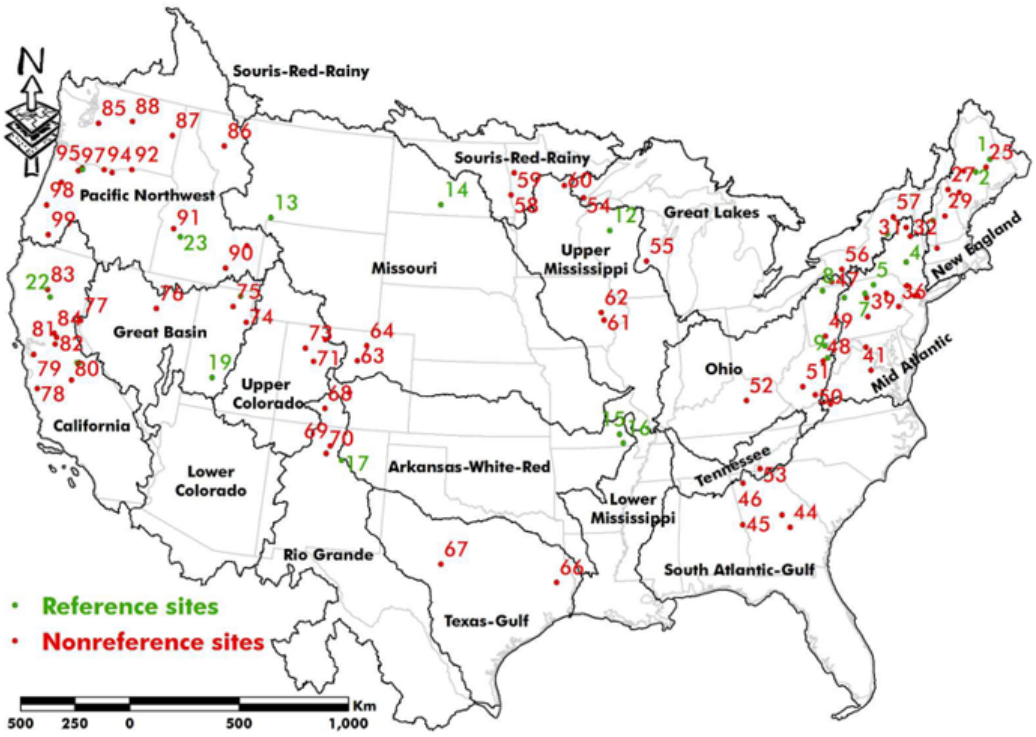

Figure 1: Geographic locations of reference (green circle) and nonreference (red circle) sites throughout the contiguous United States. The numbers are correspondent to the "ID" column in supplementary materials in Table S1. The hydrologic units (HUC02) were defined by USGS.

Partial duration series (PDS)

The PDS comprises several high flow events rather than just the largest peak flow of each year [16].To ensure compliance with the AMF assumption, it is essential that the selected floods are independent [21]. Developing a PDS from daily mean streamflow data is somewhat subjective. However, as long as the selected peaks represent independent floods and the selection process does not impose too many restrictions [51], can serve as a reliable representation of flood peaks in the region.

In this study, we initially selected flows greater than the minimum peak flow reported in the AMF. Subsequently, we identified the absolute and relative maximums. The final step involved assessing the independence of these maximums. We utilized temporal independence criteria proposed by [26], considering events spaced at least five days apart plus the natural logarithm of drainage area in square miles, as independent flooding events. The length of PDS records for each site is detailed in supplementary materials Table S1. On average, the PDS contained at least five floods in addition to the annual maximum.

Results and discussions

Performance of LP3 and GEV

The performance of a statistical distribution in estimating flood quantiles is assessed through a goodness-of-fit test [29]. When either an LP3 or GEV distribution was fitted to the AMF or PDS, Pearson cross-correlation indicated how accurately the distribution estimated floods with different recurrence intervals. Figure 2 depicts two flood frequency models and the goodness-of-fit plots for the Connecticut River at Montague City, Massachusetts (USGS 01170500). While both LP3 (Figure 2a) and GEV (Figure 2b) exhibited reliable performance, as evidenced by high correlation coefficients, both distributions missed a few low-frequency floods. This occurred because the goodness of fit primarily evaluated the relative performance of the LP3 or GEV, assigning less weight to the upper and lower tails of the distributions [52]. Therefore, the goodness-of-fit test was supplemented by the ratio (R) of observed to estimated floods to provide a more comprehensive evaluation of the performance of statistical distributions.

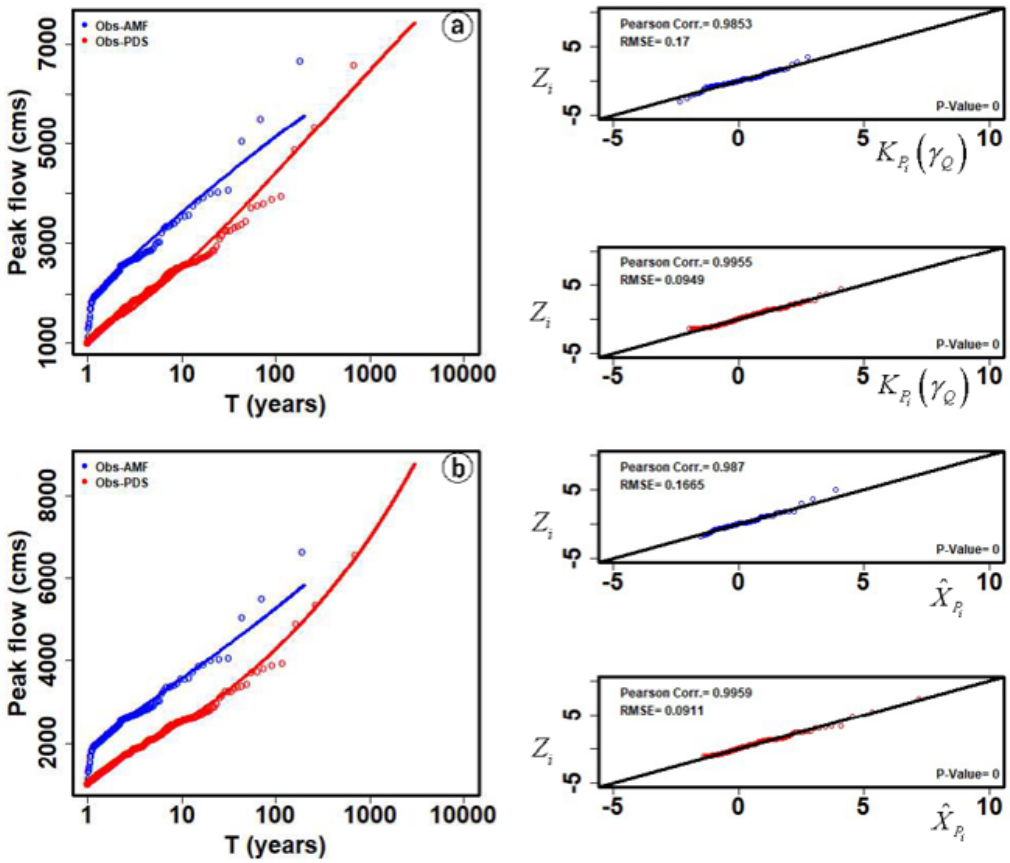

Figure 2: Flood frequency curves and goodness-of-fit developed for the Connecticut River at Montague City, MA (USGS 01170500): a) LP3 was fitted to AMF and PDS. The two plots on the right indicated correlation between observed and estimated flood quantiles for LP3 fitted to AMF (blue circles) and PDS (red circles). b) Similar to a) but for GEV.

When the ratio fell below one, the distribution performed reliably, indicating that the estimated floods exceeded the corresponding observations. Conversely, a ratio greater than one indicated underestimated flood quantiles, suggesting poor performance of the distribution. We compared the performance of LP3 and GEV with both AMF and PDS at reference and nonreference sites for floods with return periods ranging from two to 400 years. However, in case where either LP3 or GEV performed well with both AMF and PDS, preference should be given to AMF data over PDS, as the development process of a PDS series was subjective.

Two-year flood

LP3 performed well in estimating a two-year flood event with both AMF and PDS information (Figure 3a and Table 1). For regional flood analysis in the Northeast and Pacific Northwest, considering the increase in high-frequency flooding prompted by sea-level rise [53, 54], using GEV with PDS provided better quantile estimates than AMF. However, for the Upper Colorado and northeast of the Great Basin, LP3 outperformed GEV (Figure 3a). Since LP3 demonstrated similar performance with both AMF and PDS, AMF usage was preferred (Table 1). Overall, GEV reliably estimated a two-year flood with PDS information. The distinction between reference and nonreference sites did not affect the performance of LP3, while GEV was sensitive to the conditions of the study sites (Table 1).

Table 1: The ratio (R) of observed peak flows to the corresponding flood quantiles (Obs/Est) estimated by LP3 and GEV distributions for reference and nonreference sites.

	LP3				GEV			
	Reference sites (#22) [a]		Nonreference sites (#67)		Reference sites (#24)		Nonreference sites (#75)	
	AMF	PDS	AMF	PDS	AMF	PDS	AMF	PDS
T-years	R < 1 [b] (R > 1) [c]	R < 1 (R > 1)	R < 1 (R > 1)	R < 1 (R > 1)	R < 1 (R > 1)	R < 1 (R > 1)	R < 1 (R > 1)	R < 1 (R > 1)
400	--- (---)	4/22 (82%)	--- (---)	12/67 (82%)	--- (---)	20/24 (17%)	--- (---)	69/75 (8%)
200	0/22 (100%)	3/22 (86%)	0/67 (100%)	14/67 (79%)	12/24 (50%)	20/24 (17%)	43/75 (43%)	67/75 (11%)
100	1/22 (95%)	4/22 (82%)	2/67 (97%)	14/67 (79%)	14/24 (42%)	19/24 (21%)	34/75 (55%)	61/75 (19%)
50	2/22 (91%)	10/22 (55%)	2/67 (97%)	20/67 (70%)	10/24 (58%)	16/24 (33%)	38/75 (49%)	51/75 (32%)
25	6/22 (73%)	12/22 (45%)	6/67 (91%)	27/67 (60%)	10/24 (58%)	9/24 (63%)	35/75 (53%)	23/75 (69%)
10	14/22 (36%)	19/22 (14%)	42/67 (37%)	61/67 (9%)	13/24 (46%)	2/24 (92%)	44/75 (41%)	9/75 (88%)
5	22/22 (0%)	22/22 (0%)	65/67 (3%)	66/67 (1%)	13/24 (46%)	3/24 (88%)	40/75 (47%)	0/75 (100%)
2	22/22 (0%)	22/22 (0%)	66/67 (1%)	67/67 (0%)	17/24 (29%)	23/24 (4%)	39/75 (48%)	69/75 (8%)

[a] There were 24 reference and 75 nonreference sites. For LP3, there were two reference (06354000 and 08380500) and eight nonreference sites (05054000, 05079000, 06754000, 08126380, 11179000, 11446500, 12117500, and 14359000) with scale parameter β<3 that made Eq. 4 undefined. Those sites were not pursued further for LP3 analysis. [b]R < 1: flood was overestimated; R > 1: flood was underestimated [c]First numbers represent the fraction of sites with overestimated floods. The numbers in parentheses indicate the percentage of underestimated floods.

Five-year flood

LP3 performed well in estimating a five-year flood with both AMF and PDS (Figure 3b and Table 1). However, the performance of GEV was not spatially consistent. Interestingly, adding more information to a flood series through the use of the PDS alongside AMF did not improve the performance of the GEV and actually worsened it (Table 1). At equal numbers of sites, the GEV with AMF could or could not estimate floods well. Given the uncertainty surrounding the use of GEV for a five-year flood estimation, it appeared that LP3, either with AMF or PDS (with a preference for AMF), was a better choice regardless of site being reference or non-reference (Table 1).

Ten-year flood

For 10-year flooding events, the use of the PDS improved the LP3 flood quantile estimates compared to the AMF for both reference and nonreference sites (Table 1, No. of sites with R < 1 for 10-year event, $\frac{19-14}{14}=36\%$ and nonreference $\frac{61-42}{42}=45\%$) sites. Similarly to a five-year flood, the performance of GEV worsened when using the PDS instead of the AMF (Table 1). The LP3 distribution with PDS data should be utilized for both reference and nonreference sites, while the use of GEV distribution should be avoided. At three sites (nonreference: USGS 03284000-Kentucky and 09239500-Colorado; reference: USGS 04254500-New York), neither LP3 nor GEV performed well, even with the use of the PDS instead of the AMF (Figure 3c). Other distributions besides LP3 and GEV may improve flood estimations for these sites.

Twenty-five-year flood

For the return period of 25 years, LP3 showed a 100 percent improvement for reference sites when the PDS was utilized (Table 1, No. of sites with R < 1 for 25-year event, $\frac{12-6}{6}=100\%$), while for nonreference sites, the improvement was even higher ($\frac{27-6}{6}=350\%$). The performance of GEV did not change considerably when using the PDS instead of the AMF (Table 1). Overall, the performance of LP3 and GEV did not indicate a consistent spatial pattern favoring one over the other (Figure 3d). At one cluster of sites, mainly located

in the mid-Atlantic, neither LP3 nor GEV distributions performed well (Figure 3d). Since in that cluster, the number of reference sites was greater than nonreference sites, it might imply an increase in climate nonstationarity for higher flood quantiles in the Northeast [55], where LP3 and GEV failed to capture the peak flows. A smaller number of nonreference sites compared to reference sites, where neither LP3 nor GEV were fitted to peak flow observations, indicated how climate nonstationarity could be masked by anthropogenic disturbances in the northeastern U.S. [56].

Fifty-year flood

For 50-year floods, LP3 did not perform well with the AMF regardless of site conditions (Table 1). Although using the PDS improved the performance of LP3, the number of sites with R <1 and R > 1 did not indicate significant differences. LP3 might not be a suitable choice for 50-year flood estimations across the U.S. However, the GEV outperformed LP3 for estimating 50-year floods by using a PDS series instead of an AMF. The performance of GEV was enhanced for both reference (Table 1, No. of sites with R < 1 for 50-year event, $\frac{16-10}{10}=60\%$) and nonreference sites ($\frac{51-38}{38}=34\%$).

It appeared that GEV could perform well for flood estimations in the Northeast (Figure 3e). Since neither LP3 nor GEV performed well at the following nonreference sites (USGS01076500-New Hampshire, 01434000-New York, 03082500-Pennsylvania, and 08313000-New Mexico), utilizing other distributions besides LP3 and GEV is suggested (Figure 3e). With all those sites being nonreference, it might indicate that, depending on the region of interest, anthropogenic nonstationarity might echo climate nonstationarity [56].

One-hundred-year flood

For a 100-year flood, the PDS did not improve the performance of LP3 compared to AMF (Table 1). However, using the PDS instead of the AMF significantly enhanced the performance of GEV for both reference (Table 1, No. of sites with R < 1 for 100-year event, $\frac{19-14}{14}=36\%$) and nonreference ($\frac{61-34}{34}=79\%$) sites. There was a cluster of sites in the Northeast where neither LP3 nor GEV performed well in estimating a 100-year flood (Figure 3f). As mentioned earlier, this might indicate increases in climate variability stimulated by changes in sea-surface temperature (Atlantic Multi-decadal Oscillation, represented by AMO index) or sea-level pressure (North Atlantic Oscillation, represented by NAO index) [56- 59].

Two-hundred-year flood

The 200-year floods showed similar patterns to 100-year floods (Figure 3g and Table 1). The performance of LP3 was not significantly improved, even when using the PDS instead of the AMF. However, the PDS enhanced the performance of the GEV for both reference (Table 1, No. of sites with R < 1 for a 200-year event, $\frac{20-12}{12}=67\%$) and nonreference sites ($\frac{67-43}{43}=56\%$). At six sites (Figure 3g), mostly nonreference, both LP3 and GEV did not estimate floods well (nonreference: USGS 01170500-Massachusetts and 01567000-Pennsylvania; reference: USGS 03069500-West Virginia, 05454500-Iowa, 05464500-Iowa, and 06714000-Colorado). For longer return periods, climate or anthropogenic nonstationarity indicated greater effects on flood quantile estimates. However, using the PDS helped the GEV better estimate a 200-yr flood.

Four-hundred-year flood

Flood frequency analysis for a return period of 400 years was only feasible for the PDS since it comprised of at least 350 peak flow observations on average (Table S1). Regardless of whether the sites were reference or nonreference, the GEV considerably better estimated a 400-year flood than the LP3 (Figure 3h and Table 1). At a cluster of sites in the mid-Atlantic, neither GEV nor LP3 accurately estimate a 400-year flood, even when using the PDS instead of the AMF. Similar to a 200-year flood, the confounding effects of changing climate and anthropogenic disturbances were evident in the Northeast, suggesting greater uncertainties in high flood quantile forecasting.

Summary and conclusions

We constructed a PDS from daily streamflow data gathered from 24 reference and 75 nonreference sites across the U.S., each site having more than 100 years of AMF records. Since the PDS provided multiple flooding events per year instead of just the maximum observed peak flow as indicated by the AMF, its inclusion in flood frequency analysis suggested potential improvement in flood quantile estimates. We applied LP3 (product moment) and GEV (L-moment) distributions to both the AMF and PDS. By comparing results between reference and nonreference sites, we aimed to differentiate between climate variations with anthropogenic nonstationarity.

We have summarized the results for distributions suitable for estimating two- to 400-year flooding events in Table 2. We observed that for high-frequency floods with recurrence intervals of two to 10 years, LP3 fitting to the AMF data performed well. However, for longer return periods, the PDS aided in improving the performance of LP3. There was no clear recommendation for an appropriate distribution for a 25-year flood. It appears this return period acted as a transition, replacing the LP3, which reliably estimated shorter period floods of two to 10 years, with the GEV for estimating longer period flooding events. For high flood quantiles of 50-400 years, the performance of GEV was significantly enhanced using the PDS.

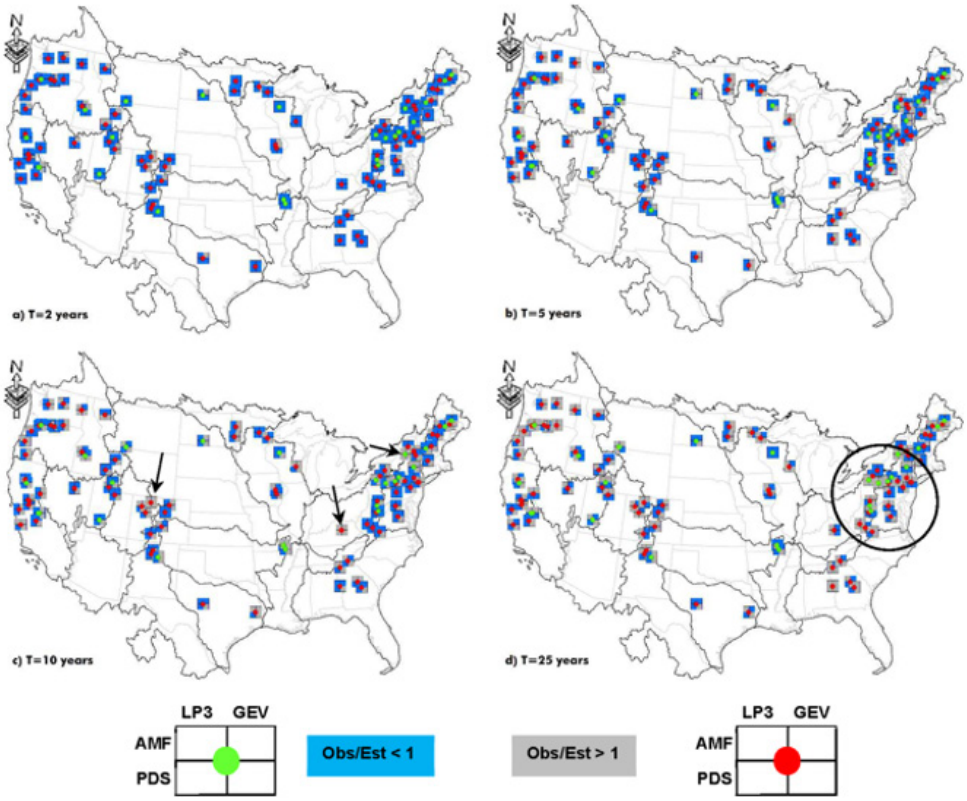

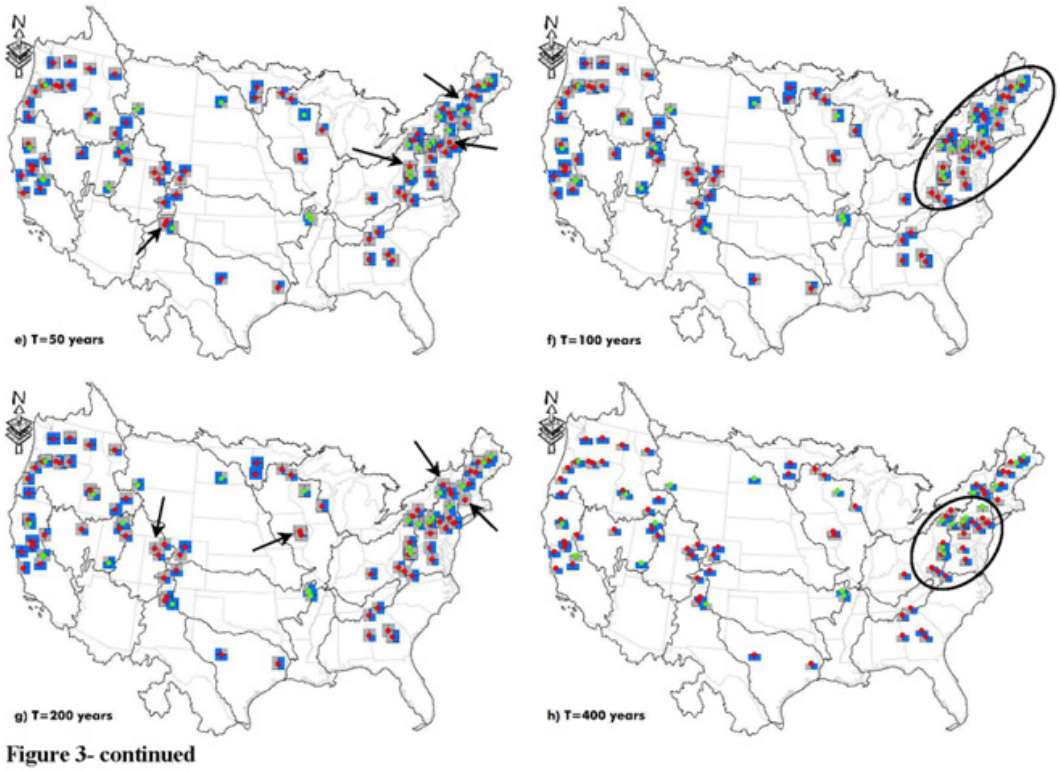

Figure 3- continued

Figure 3 a-h: Performance of LP3 and GEV distributions in estimating flood quantiles of two to 400 years recurrence intervals. The left column of the box belongs to LP3 while the right side represents GEV. The first and second rows describe results for AMF and PDS, respectively. The green circle in the middle of the box indicates a reference site while the red circle belongs to a nonreference site. Blue and gray themes represent R < 1 and R > 1, respectively. Arrows and circles on the maps emphasize locations where neither LP3 nor GEV provided reliable flood quantiles estimates.

Table 2: Suggested statistical distribution along with appropriate peak flow information for improving flood quantiles estimates across the U.S.

T-years	Choice of distribution
400	GEV PDS
200	GEV PDS
100	GEV PDS
50	GEV PDS
25	No specific pattern, potential transition period from LP3 to GEV
10	LP3 with PDS
5	LP3 with AMF/PDS
2	LP3 with AMF/PDS

Sites where neither LP3 nor GEV reliably estimated flood quantiles require special attention. This could be indicative of increases in either climate or anthropogenic nonstationarity in the region. One potential solution would be to examine the performance of other distributions introduced for addressing nonstationarity [57]. Poor performance of LP3 or GEV was mainly observed in the Northeast, where climate nonstationarity has affected high flood quantiles in the region [54]. Increases in climate variability could be stimulated by Atlantic circulation patterns [58-61]. Future study should focus on understanding how variations in flood generating mechanisms can affect high and low flood quantile estimates. Reliable flood quantile estimates, considering nonstationarity, help improve flood forecasting, and reduce property damage and loss of life through enhanced infrastructure design, reservoir management, and floodplain determination.

Acknowledgments

Authors would like to acknowledge and extent their gratitude for the support provided by Kansas State University for the current research. The work was conducted from 2018 to 2019, during Dr. Berton's tenure as a postdoctoral fellow and Dr. Rahmani's tenure as an assistant professor in the Department of Biological and Agricultural Engineering at Kansas State University.

Conflict of Interest

No Conflict of Interest

Disclaimers

The views expressed in this publication are solely those of the authors and do not necessarily reflect the views of their either formers or current affiliations.

References

1. Basso S, Schirmer M, Botter G (2016) A physically based analytical model of flood frequency curves. Geophysical Research Letters 43: 9070-9076.
2. Jakob D (2013) Nonstationarity in Extremes and Engineering Design, in: AghaKouchak A, Easterling D, Hsu K, Schubert S, Sorooshian S (Eds.), Extremes in a Changing Climate: Detection, Analysis and Uncertainty, Water Science and Technology Library. Springer, Dordrecht, pp. 363-417.
3. Keller L, Rössler O, Martius O, Weingartner R (2018) Delineation of flood generating processes and their hydrological response. Hydrological Processes 32: 228-240.
4. Read LK, Vogel RM (2015) Reliability, return periods, and risk under nonstationarity. Water Resources Research 51: 6381-6398.
5. Rosner A, Vogel RM, Kirshen PH (2014) A risk-based approach to flood management decisions in a nonstationary world. Water Resources Research 50: 1928-1942.
6. Yan L, Xiong L, Guo S, Xu CY, Xia J, et al. (2017a) Comparison of four nonstationary hydrologic design methods for changing environment. Journal of Hydrology 551: 132-150.
7. England Jr JF, Cohn TA, Faber BA, Stedinger JR, Thomas Jr WO, et al. (2018) Guidelines for determining flood flow frequency—Bulletin 17C (Report No. 4-B5). Techniques and Methods Reston, VA.
8. Shaw SB, Walter MT (2011) Using comparative analysis to teach about the nature of nonstationarity in future flood predictions. Hydrol. Earth Syst. Sci. Discuss 8: 11387-11411.
9. Yan L, Xiong L, Liu D, Hu T, Xu CY (2017b) Frequency analysis of nonstationary annual maximum flood series using the time-varying two-component mixture distributions: Time-varying Two-component Mixture Distributions. Hydrological Processes 31: 69-89.
10. Luke A, Vrugt JA, AghaKouchak A, Matthew R, Sanders BF (2017) Predicting nonstationary flood frequencies: Evidence supports an updated stationarity thesis in the United States. Water Resources Research 53: 5469-5494.
11. Milly PCD, Betancourt J, Falkenmark M, Hirsch RM, Kundzewicz ZW, et al. (2008) Stationarity is dead: Whither water management? Science 319: 573-574.
12. Slater LJ, Singer MB, Kirchner JW (2015) Hydrologic versus geomorphic drivers of trends in flood hazard. Geophysical Research Letters 42: 370-376.
13. Stephens E, Day JJ, Pappenberger F, Cloke H (2015) Precipitation and floodiness. Geophysical Research Letters 42: 10316-10323.
14. Vasiliades L, Galiatsatou P, Loukas A (2015) Nonstationary Frequency Analysis of Annual Maximum Rainfall Using Climate Covariates. Water Resources Management 29: 339-358.
15. Yan M, Liu J, Wang, Z (2017) Global Climate Responses to Land Use and Land Cover Changes Over the Past Two Millennia. Atmosphere 8: 64.
16. Lang M, Ouarda TBMJ, Bobée B (1999) Towards operational guidelines for over-threshold modeling. Journal of Hydrology 225: 103-117.
17. Roth M, Buishand TA, Jongbloed G, Klein Tank AMG, van Zanten JH (2012). A regional peaks-over-threshold model in a nonstationary climate. Water Resources Research 48.
18. Adamowski K, Liang GC, Patry GG (1998) Annual maxima and partial duration flood series analysis by parametric and non-parametric methods. Hydrological Processes 12: n1685-1699.
19. Archfield SA, Hirsch RM, Viglione A, Blöschl G (2016) Fragmented patterns of flood change across the United States. Geophysical Research Letters 43: 10232-10239.

20. Armstrong WH, Collins MJ, Snyder NP (2012) Increased frequency of low-magnitude floods in New England. Journal of the American Water Resources Association 48: 306-320.

21. Bezak N, Brilly M, Šraj M (2014) Comparison between the peaks-over-threshold method and the annual maximum method for flood frequency analysis. Hydrological Sciences Journal 59: 959-977.

22. Burn DH, Whitfield PH (2017) Changes in cold region flood regimes inferred from long-record reference gauging stations. Water Resources Research 53: 2643-2658.

23. Keast D, Ellison J (2013) Magnitude Frequency Analysis of Small Floods Using the Annual and Partial Series. Water 5: 1816-1829.

24. Chou C, Chiang JCH, Lan CW, Chung CH, Liao YC, et al. (2013) Increase in the range between wet and dry season precipitation. Nature Geoscience 6: 263-267.

25. Seager R, Naik N, Vogel L (2011) Does Global Warming Cause Intensified Interannual Hydroclimate Variability? J. Climate 25: 3355-3372.

26. Flynn KM (1982) Guidelines for determining flood flow frequency—Bulletin 17B. U.S. Geological Survey, Office of Water Data Coordination, Reston, Virginia.

27. Langbein WB (1949) Annual floods and the partial-duration flood series. Eos, Transactions American Geophysical Union 30: 879-881.

28. Nied M, Pardowitz T, Nissen K, Ulbrich U, Hundecha Y, et al. (2014). On the relationship between hydro-meteorological patterns and flood types. Journal of Hydrology 519: 3249-3262.

29. Serago JM, Vogel RM (2018) Parsimonious nonstationary flood frequency analysis. Advances in Water Resources 112: 1-16.

30. Villarini G, Smith JA, Baeck ML, Krajewski WF (2011) Examining Flood Frequency Distributions in the Midwest U.S. JAWRA Journal of the American Water Resources Association 47: 447-463.

31. Berghuijs WR, Woods RA, Hutton CJ, Sivapalan M (2016) Dominant flood generating mechanisms across the United States Geophysical Research Letters 43: 4382-4390.

32. Maurer EP, Kayser G, Doyle L, Wood AW (2018) Adjusting Flood Peak Frequency Changes to Account for Climate Change Impacts in the Western United States. Journal of Water Resources Planning and Management 144: 1-12.

33. Slater LJ, Villarini G (2016) Recent trends in U.S. flood risk. Geophysical Research Letters 43: 12428-12436.

34. Vogel RM, Wilson I (1996) Probability distribution of annual maximum, mean, and minimum stream flows in the united states. Journal of Hydrologic Engineering 1: 69-76.

35. Slater LJ, Villarini G (2018) Enhancing the Predictability of Seasonal Streamflow With a Statistical-Dynamical Approach. Geophysical Research Letters 45: 6504-6513.

36. Wang W, Lu H, Ruby Leung L, Li HY, Zhao J, et al. (2017) Dam Construction in Lancang-Mekong River Basin Could Mitigate Future Flood Risk From Warming-Induced Intensified Rainfall: Dam Mitigate Flood Risk in Mekong. Geophysical Research Letters 44: 10378-10386.

37. Bureau of Reclamation & USACE (2015) Probabilistic Hydrologic Hazard Analysis, in: Best Practices in Dam and Levee Safety Risk Analysis, Training Manual. The Bureau of Reclamation Technical Service Center and the U.S. Army Corps of Engineers Risk Management Center, Denver, Co, p. 20.

38. Micevski T, Hackelbusch A, Haddad K, Kuczera G, Rahman A (2015) Regionalisation of the parameters of the log-Pearson 3 distribution: a case study for New South Wales, Australia. Hydrological Processes 29: 250-260.

39. Sraj M, Bezak N, Brilly M (2014) Bivariate flood frequency analysis using the copula function: a case study of the Litija station on the Sava River. Hydrological Processes 29: 225-238.

40. Bobée B (1975) The Log Pearson type 3 distribution and its application in hydrology. Water Resources Research 11: 681-689.

41. Griffis VW, Stedinger JR (2007) Log-Pearson Type 3 Distribution and Its Application in Flood Frequency Analysis. I: Distribution Characteristics. Journal of Hydrologic Engineering 12: 482-491.

42. Madsen H, Rasmussen PF, Rosbjerg D (1997) Comparison of annual maximum series and partial duration series methods for modeling extreme hydrologic events: 1. At-site modeling. Water Resources Research 33: 747-757.

43. Vogel RM, Fennessey NM (1993) L moment diagrams should replace product moment diagrams. Water Resources Research 29: 1745-1752.

44. Stedinger JR, Vogel RM, Foufoula Georgiou E (1993) Frequency analysis of extreme events, in: Maidment, D.R. (Ed.), Handbook of Hydrology. McGraw-Hill, the University of Michigan, p. 1424.

45. Blom G (1958) Statistical estimates and transformed beta-variables. John Wiley & Sons, Inc.

46. Cunnane C (1978) Unbiased plotting positions — A review. Journal of Hydrology 37: 205-222.

47. Falcone J, (2011) GAGES-II: Geospatial attributes of gages for evaluating streamflow (vector digital data). U.S. Geological Survey, Reston, Virginia.

48. Lins HF (2012) USGS Hydro-Climatic Data Network 2009 (HCDN–2009) (Fact Sheet). U. S. Geological Survey, Reston, VA.

49. Hirsch RM, De Cicco LA (2015) User guide to Exploration and Graphics for RivEr Trends (EGRET) and dataRetrieval: R packages for hydrologic data, Techniques and Methods. U.S. Geological Survey, Reston, VA.

50. Wickham H, François R, Henry L, Müller K (2018) dplyr: A Grammar of Data Manipulation, R package version 0.7.6.

51. Fahim A, Jean, R (1983) The effect of certain restrictions imposed on the interarrival times of flood events on the Poisson distribution used for modeling flood counts. Water Resources Research 19: 481-485.

52. Alila Y, Mtiraoui A (2002) Implications of heterogeneous flood-frequency distributions on traditional stream-discharge prediction techniques. Hydrological Processes 16: 1065-1084.

53. Moftakhari HR, AghaKouchak A, Sanders BF, Feldman DL, Sweet W, et al. (2015) Increased nuisance flooding along the coasts of the United States due to sea level rise: Past and future. Geophysical Research Letters 42: 9846-9852.

54. Moftakhari HR, AghaKouchak A, Sanders BF, Allaire M, Matthew RA (2018) What Is Nuisance Flooding? Defining and Monitoring an Emerging Challenge. Water Resources Research. 54: 4218-4227.

55. Collins MJ (2009) Evidence for changing flood risk in New England since the late 20th century. Journal of the American Water Resources Association 45: 279-290.

56. Berton R, Driscoll CT, Chandler DG (2016) Changing climate increases discharge and attenuates its seasonal distribution in the northeastern United States. Journal of Hydrology: Regional Studies 5: 164-178.

57. Salas J, Obeysekera J (2013) Revisiting the Concepts of Return Period and Risk for Nonstationary Hydrologic Extreme Events. Journal of Hydrologic Engineering 19: 554-568.

58. Berton R, Driscoll CT, Adamowski JF (2017) The near-term prediction of drought and flooding conditions in the northeastern United States based on extreme phases of AMO and NAO. Journal of Hydrology 553: 130-141.

59. Collins MJ, Kirk JP, Pettit J, DeGaetano AT, McCown ZS, et al. (2014) Annual floods in New England (USA) and Atlantic Canada: synoptic climatology and generating mechanisms. Physical Geography 35: 195-219.

60. Hurrell JW, Deser C (2009) North Atlantic climate variability: The role of the North Atlantic Oscillation. Journal of Marine Systems 78: 28-41.

61. Tootle GA, Piechota TC, Singh A (2005) Coupled oceanic-atmospheric variability and U.S. streamflow. Water Resources Research 41: W12408.

Table S1: Description of 24 reference and 75 nonreference study sites with more than 100 years of peak flow information across the contiguous United States.

No.	ID	USGS streamflow gauging stations	Latitude	Longitude	Period of record	No. of observed AMF (PDS)	Drainage area (km²)	Gauge height (m)	Site condition
1	1030500	Mattawamkeag River near Mattawamkeag, ME	45.5	-68.31	1903-2015	115 (316)	3,673	66	Reference
2	1031500	Piscataquis River near Dover-Foxcroft, ME	45.18	-69.31	1903-2015	115 (412)	772	109	Reference
3	1144000	White River at West Hartford, VT	43.71	-72.42	1916-2017	102 (414)	1,787	114	Reference
4	1350000	Schoharie Creek at Prattsville, NY	42.32	-74.44	1903-2017	109 (344)	614	345	Reference
5	1532000	Towanda Creek near Monroeton, PA	41.71	-76.48	1914-2016	104 (254)	557	233	Reference
6	1543000	Driftwood Br Sinnemahoning Cr at Sterling Run, PA	41.41	-78.2	1914-2017	104 (362)	704	273	Reference
7	1550000	Lyoming Creek near Trout Run, PA	41.42	-77.03	1914-2017	104 (278)	448	212	Reference
8	3015500	Brokenstraw Creek at Youngsville, PA	41.85	-79.32	1910-2017	108 (363)	831	362	Reference
9	3069500	Cheat River near Parsons, WV	39.12	-79.68	1844-2016	106 (267)	1,870	485	Reference
10	3070500	Big Sandy Creek at Rockville, WV	39.62	-79.7	1888-2016	105 (197)	518	403	Reference
11	4254500	Moose Rover at Mckeever, NY	43.61	-75.11	1869-2017	103 (125)	940	451	Reference
12	5362000	Jump River at Sheldon, WI	45.31	-90.96	1916-2016	102 (372)	1,492	333	Reference
13	6191500	Yellowstone River at Corwin Springs, MT	45.11	-110.79	1890-2017	111 (287)	6,775	1548	Reference
14	6354000	Cannonball River at Breien, ND	46.38	-100.93	1906-2017	102 (588)	10,619	511	Reference
15	7067000	Current River at Van Buren, MO	36.99	-91.01	1904-2017	106 (422)	4,318	135	Reference
16	7068000	Current River at Doniphan, MO	36.62	-90.85	1904-2017	101 (448)	5,278	98	Reference
17	8380500	Gallinaz Creek near Montezuma, NM	35.65	-105.32	1915-2016	100 (468)	218	2097	Reference
18	10109001	Com F Logan R AB ST D and Cache HL Can NR Logan, UT	41.74	-111.78	1896-2017	122 (702)	554	1426	Reference
19	10234500	Beaver River near Beaver, UT	38.28	-112.57	1914-2017	104 (632)	236	1890	Reference
20	11264500	Merced R A Happy Isles Bridge NR Yosemite, CA	37.73	-119.56	1916-2017	102 (443)	469	1228	Reference
21	11266500	Merced R A Pohono Bridge NR Yosemite, CA	37.72	-119.67	1917-2017	101 (406)	831	1177	Reference
22	11383500	Deer C NR Vina, CA	40.01	-121.95	1912-2017	101 (725)	539	146	Reference
23	13185000	Boise River NR Twin Springs, ID	43.66	-115.73	1871-2015	109 (561)	2,155	1018	Reference
24	14137000	Sandy River near Marmot, OR	45.4	-122.14	1912-2015	106 (513)	684	0	Reference
25	1034500	Penobscot River at West Enfield, ME	45.24	-68.65	1902-2017	116 (435)	16,633	38	Non reference
26	1042500	Kennebec River at The Forks, ME	45.34	-69.96	1901-2017	116 (710)	4,118	173	Non reference
27	1053500	Androscoggin River at Errol, NH	44.78	-71.13	1906-2017	112 (903)	2,709	374	Non reference
28	1054500	Androscoggin River at Rumford, ME	44.55	-70.54	1893-2017	125 (477)	5,356	128	Non reference
29	1076500	Pemigewasset River at Plymouth, NH	43.76	-71.69	1904-2017	114 (341)	1,611	139	Non reference
30	1170500	Connecticut River at Montague City, MA	42.58	-72.57	1904-2017	114 (424)	20,357	30	Non reference
31	1315500	Hudson River at North Creek, NY	43.7	-73.98	1908-2017	110 (325)	2,051	301	Non reference
32	1325000	Sacandaga River at Stewarts Bridge NR Hadley, NY	43.31	-73.87	1908-2017	110 (291)	2,732	177	Non reference

33	1381000	Rockaway River below Reservoir at Boonton, NJ	40.9	-74.39	1903-2017	106 (1208)	308	60	Non reference
34	1389500	Passaic River at Little Falls, NJ	40.88	-74.23	1810-2017	125 (753)	1,974	37	Non reference
35	1434000	Delaware River at Port Jervis, NY	41.37	-74.7	1903-2017	114 (410)	7,951	126	Non reference
36	1453000	Lehigh River at Bethlehem, PA	40.62	-75.38	1902-2017	112 (342)	3,313	64	Non reference
37	1536500	Susquehanna River at Wilkes-Barre, PA	41.25	-75.88	1786-2017	132 (455)	25,796	156	Non reference
38	1551500	WB Susquehanna River at Williamsport, PA	41.24	-77	1889-2017	124 (418)	14,716	151	Non reference
39	1567000	Juniata River at Newport, PA	40.48	-77.13	1889-2017	120 (487)	8,687	111	Non reference
40	1638500	Potomac River at Point of Rocks, MD	39.27	-77.54	1889-2017	124 (530)	24,996	61	Non reference
41	1668000	Rappahannock River NR Fredericksburg, VA	38.31	-77.53	1908-2017	110 (752)	4,131	21	Non reference
42	2055000	Roanoke River at Roanoke, VA	37.26	-79.94	1889-2017	120 (540)	995	276	Non reference
43	2223000	Oconee River at Milledgeville, GA	33.09	-83.22	1904-2017	115 (680)	7,640	70	Non reference
44	2223500	Oconee River at Dublin, GA	32.54	-82.89	1894-2017	124 (806)	11,396	45	Non reference
45	2339500	Chattahoochee River at West Point, GA	32.89	-85.18	1897-2017	122 (693)	9,194	168	Non reference
46	2387500	Oostanaula River at Resaca, GA	34.58	-84.94	1886-2017	127 (738)	4,149	184	Non reference
47	3011020	Allegheny River at Salamanca, NY	42.16	-78.72	1904-2017	114 (419)	4,165	414	Non reference
48	3051000	Tygart Valley River at Belington, WV	39.03	-79.94	1908-2017	111 (397)	1,052	512	Non reference
49	3082500	Youghiogheny River at Connellsville, PA	40.02	-79.59	1860-2017	128 (463)	3,434	262	Non reference
50	3183500	Greenbrier River at Alderson, WV	37.72	-80.64	1896-2017	122 (443)	3,533	466	Non reference
51	3193000	Kanawha River at Kanawha Falls, WV	38.14	-81.21	1878-2017	140 (560)	21,681	189	Non reference
52	3284000	Kentucky River at Lock 10 NR Winchester, KY	37.89	-84.26	1908-2017	109 (484)	10,243	170	Non reference
53	3548500	Hiwassee River above Murphy, NC	35.08	-84	1897-2017	107 (332)	1,052	469	Non reference
54	4024000	St. Louis River at Scanlon, MN	46.7	-92.42	1908-2017	110 (547)	8,884	336	Non reference
55	4073500	Fox River at Berlin, WI	43.95	-88.95	1898-2017	118 (781)	3,471	227	Non reference
56	4223000	Genesee River at Portageville, NY	42.57	-78.04	1902-2017	109 (258)	2,549	329	Non reference
57	4266500	Raquette River at Piercefield, NY	44.23	-74.57	1900-2017	110 (374)	1,867	458	Non reference
58	5054000	Red River of the North at Fargo, ND	46.86	-96.78	1897-2017	116 (1146)	17,612	263	Non reference
59	5079000	Red Lake River at Crookston, MN	47.78	-96.61	1897-2017	117 (985)	13,649	254	Non reference
60	5211000	Mississippi River at Grand Rapids, MN	47.23	-93.53	1884-2017	134 (1928)	8,728	379	Non reference
61	5454500	Iowa River at Iowa City, IA	41.66	-91.54	1881-2017	117 (996)	8,472	188	Non reference

62	5464500	Cedar River at Cedar Rapids, IA	41.97	-91.67	1903-2016	116 (925)	16,861	214	Non reference
63	6714000	South Platte River at Denver, CO	39.76	-105	1895-2007	110 (279)	10,013	1572	Non reference
64	6754000	South Platte River Near Kersey, CO	40.41	-104.56	1902-2007	104 (965)	25,022	1395	Non reference
65	7096000	Arkansas River at Canon City, CO	38.43	-105.26	1889-2017	129 (1107)	8,073	1628	Non reference
66	8033500	Neches River NR Rockland, TX	31.03	-94.4	1904-2017	113 (998)	9,417	27	Non reference
67	8126380	Colorado River NR Ballinger, TX	31.72	-100.03	1908-2017	110 (1259)	42,367	490	Non reference
68	8220000	Rio Grande NR Del Norte, CO	37.69	-106.46	1890-2017	128 (864)	3,419	2432	Non reference
69	8279500	Rio Grande at Embudo, NM	36.21	-105.96	1889-2017	120 (800)	26,936	1765	Non reference
70	8313000	Rio Grande at Otowi Bridge, NM	35.87	-106.14	1895-2017	116 (509)	37,037	1673	Non reference
71	9085000	Roaring Fork River at Glenwood Springs, CO	39.54	-107.33	1906-2017	110 (406)	3,763	1744	Non reference
72	9239500	Yampa River at Steamboat Springs, CO	40.48	-106.83	1904-2017	111 (355)	1,469	2041	Non reference
73	9304500	White River NR Meeker, CO	40.03	-107.86	1901-2017	109 (354)	1,968	1920	Non reference
74	10128500	Weber River NR Oakley, UT	40.74	-111.25	1905-2017	113 (316)	420	2024	Non reference
75	10141000	Weber River NR Plain City, UT	41.28	-112.09	1905-2017	113 (989)	5,390	1282	Non reference
76	10322500	Humboldt River at Palisade, NV	40.61	-116.2	1903-2017	111 (732)	13,087	1472	Non reference
77	10346000	Truckee River at Farad, CA	39.43	-120.03	1900-2017	118 (667)	2,414	1571	Non reference
78	11152000	Arroyo Seco NR Soledad, CA	36.28	-121.32	1906-2017	112 (383)	632	103	Non reference
79	11179000	Alameda Creek NR Niles, CA	37.59	-121.96	1892-2017	126 (1504)	1,639	26	Non reference
80	11251000	San Joaquin River BL Friant, CA	36.98	-119.72	1908-2017	108 (1419)	4,341	90	Non reference
81	11323500	Mokelumne River BL Camanche Dam, CA	38.23	-121.02	1905-2017	114 (1345)	1,608	25	Non reference
82	11335000	Cosumnes River at Michigan Bar, CA	38.5	-121.05	1907-2017	111 (1032)	1,388	51	Non reference
83	11377100	Sacramento River Ab Bend Bridge NR Red Bluff, CA	40.29	-122.19	1879-2017	136 (897)	23,051	87	Non reference
84	11446500	American River at Fair Oaks, CA	38.64	-121.23	1862-2017	113 (1197)	4,890	22	Non reference
85	12117500	Cedar River NR Landsburg, WA	47.39	-121.95	1896-2017	118 (751)	313	172	Non reference
86	12372000	Flathead River NR Polson, MT	47.68	-114.25	1908-2017	111 (472)	18,335	821	Non reference
87	12422500	Spokane River at Spokane, WA	47.66	-117.45	1891-2017	127 (669)	11,111	517	Non reference
88	12452500	Chelan River at Chelan, WA	47.83	-120.01	1904-2015	110 (988)	2,393	327	Non reference
89	13056500	Henrys Fork NR Rexburg, ID	43.83	-111.91	1909-2017	109 (1081)	7,563	1465	Non reference
90	13077000	Snake River at Neeley, ID	42.77	-112.88	1906-2017	112 (649)	35,224	1293	Non reference

91	13247500	Payette River NR Horseshoe Bend, ID	43.94	-116.2	1906-2017	109 (829)	5,750	800	Non reference
92	14033500	Umatilla River NR Umatilla, OR	45.9	-119.33	1904-2017	114 (468)	5,931	101	Non reference
93	14048000	John Day River at Mcdonald Ferry, OR	45.59	-120.41	1905-2017	112 (562)	19,632	120	Non reference
94	14103000	Deschutes River at Moody, NR Biggs, OR	45.62	-120.91	1897-2017	113 (869)	27,195	51	Non reference
95	14140000	Bull Run River NR Bull Run (River Only), OR	45.44	-122.18	1908-2017	102 (389)	277	173	Non reference
96	14174000	Willamette River at Albany, OR	44.64	-123.11	1861-2017	133 (817)	12,536	51	Non reference
97	14210000	Clackamas River at Estacada, OR	45.3	-122.35	1909-2017	109 (594)	1,738	87	Non reference
98	14321000	Umpqua River NR Elkton, OR	43.59	-123.56	1906-2016	111 (638)	9,539	28	Non reference
99	14359000	Rogue River at Raygold NR Central Point, OR	42.44	-122.99	1906-2016	112 (798)	5,317	342	Non reference